Check for updates

Advanced Materials Technologies

ADVANCED MATERIALS TECHNOLOGIES
www.advmattechnol.com

RESEARCH ARTICLE OPEN ACCESS

A Direction-Aware Piezo-Transmittance Strain Sensor via Engineered Alignment of Carbon Nanotubes (CNTs)

Byeongmin Kang[1,2] | Kwangjun Kim[3] | Jimin Gu[4] | Junseong Ahn[5] | Yongrok Jeong[6] | Ji-Hwan Ha[7] | Sohee Jeon[2] | Soonhyoung Hwang[2] | Byung-Ho Kang[1,2] | Jihyeon Ahn[1,2] | Jong-An Choi[1,2] | Minwook Kim[3] | Yeonguk Jung[1,2] | Jun-Ho Jeong[2] | Jong G. Ok[8] | Inkyu Park[1]

[1]Department of Mechanical Engineering, Korea Advanced Institute of Science and Technology, Daejeon, Republic of Korea | [2]Nano Lithography and Manufacturing Research Center, Korea Institute of Machinery and Materials, Daejeon, Republic of Korea | [3]Department of Mechanical and Automotive Engineering, Seoul National University of Science and Technology, Seoul, Republic of Korea | [4]Department of Mechanical Engineering, University of California, Berkeley, California, USA | [5]Department of Electro-Mechanical Systems Engineering, Korea University, Sejong, Republic of Korea | [6]School of Mechanical Engineering, Kyungpook National University, Daegu, Republic of Korea | [7]Department of Mechanical Engineering, Hanbat National University, Daejeon, Republic of Korea | [8]School of Mechanical System Engineering, Seoul National University of Science and Technology, Seoul, Republic of Korea

Correspondence: Jun-Ho Jeong (jhjeong@kimm.re.kr) | Jong G. Ok (jgok@seoultech.ac.kr) | Inkyu Park (inkyu@kaist.ac.kr)

Received: 18 February 2026 | **Revised:** 8 May 2026 | **Accepted:** 2 June 2026

Keywords: anisotropic structure | carbon nanotubes | direction-aware sensing | piezo-transmittance | strain sensor | wearable electronics

ABSTRACT

Stretchable and flexible strain sensors are essential components for next-generation wearable devices and human–machine interfaces. Among various approaches, piezo-transmittance-based strain sensors offer fast response and environmental stability. However, achieving both high sensitivity and precise directional decoupling remains a significant challenge. While sensors relying on random microcracks exhibit high gauge factors, their stochastic nature hinders axis-specific sensing. On the other hand, engineered macroscopic structures like metamaterials provide structural predictability, yet they often suffer from reduced sensitivity and notable mechanical crosstalk between orthogonal axes. In this study, a direction-aware piezo-transmittance strain sensor was developed by engineering a controlled linear gap-opening mechanism in an aligned carbon nanotubes (CNTs)/polydimethylsiloxane (PDMS) composite. The uniform gap-opening structure overcomes the limitations of traditional crack-based sensors, achieving enhanced directionality, high sensitivity (gauge factor ≈ 283), low detection limit (0.03%), and excellent sensor-to-sensor uniformity (relative standard deviation < 12%). The sensor exhibits reliable performance over 17,621 strain cycles and enables precise multi-directional strain sensing through sensor arrays that quantitatively decouple orthogonal strain components. Finally, the developed sensor was integrated into wearable platforms, including attachment to joints and incorporation into stretchable exercise bands, demonstrating its potential for real-time human motion monitoring and for integration into wearable fitness and rehabilitation devices.

1 | Introduction

Stretchable and flexible strain sensors have emerged as key components for next-generation wearable devices, healthcare monitoring systems, and human–machine interface technologies [1–4]. These sensors, designed to conform to the contour of soft and curved surfaces, are particularly suited for detecting complex human motions due to their mechanical

Byeongmin Kang, Kwangjun Kim and Jimin Gu contributed equally to this work.

This is an open access article under the terms of the Creative Commons Attribution License, which permits use, distribution and reproduction in any medium, provided the original work is properly cited.
© 2026 The Author(s). *Advanced Materials Technologies* published by Wiley-VCH GmbH

compliance and adaptability. Various types of stretchable strain sensors have been developed to meet these demands, including piezoresistive, piezocapacitive, and optical transmittance-based approaches [4–13].

Among these, optical transmittance-based physical sensors detect mechanical deformation by monitoring changes in light transmission through the sensing medium [14–16]. This category includes various strategies such as piezo-transmittance mechanisms, interference-based detection, and waveguide-based designs. In particular, piezo-transmittance strain sensors operate by modulating light transmittance via mechanically induced opening or closing of micro- or nano-scale gaps within a composite structure—allowing for direct optical readout of strain without reliance on electrical resistance changes. This optical approach offers unique advantages, including fast response/recovery speeds, high sensitivity, small hysteresis, long-term stability, and strong resistance to environmental disturbances such as temperature and humidity variations. These features make piezo-transmittance mechanisms especially promising for applications requiring stable, high-fidelity strain monitoring.

However, despite these strengths, existing piezo-transmittance strain sensors face critical limitations [17–19]. Traditional designs often rely on random crack generation and propagation within carbon nanotube (CNT)-based elastomer composites to generate optical modulation under strain. This inherently causes poor control over crack initiation and propagation, leading to unpredictable and non-uniform strain responses, poor directionality, and high sensor-to-sensor variability. This inherent randomness complicates calibration, limits reproducibility, and undermines the sensor's ability to reliably resolve multi-directional strains.

Recent studies have explored strategies to improve reliability, such as enhancing the mechanical stability of CNT networks or incorporating fracture-arresting architectures [20–22]. These advances have contributed to improvements in strain-response predictability and structural control through engineering of designed deformation pathways. Nevertheless, two critical challenges remain: (i) achieving precise control over strain directionality [23–26], and (ii) preserving signal fidelity under complex, dynamic skin deformations [27–31]. Addressing these challenges is essential for realizing truly practical, real-world deployable piezo-transmittance strain sensors.

To overcome these challenges, we introduce a direction-aware piezo-transmittance strain sensor based on a controlled, uniform gap-opening mechanism realized through engineered alignment of CNTs within a polydimethylsiloxane (PDMS) matrix. By replacing stochastic crack formation with deterministic, anisotropic structural deformation, our sensor achieves enhanced directionality, improved reproducibility, and reliable multi-directional strain detection. Furthermore, by systematically studying the effect of CNT aspect ratio on mechanical and optical properties, we optimized the composite structure to achieve a balance between stretchability, sensitivity, and uniformity. Moreover, by enabling direct skin attachment without the need for intermediary garments or protective structures, the developed sensor offers a practical advancement toward stable, skin-conformal strain monitoring under dynamic conditions. Through these applications, we demonstrate the sensor's suitability for the precise monitoring of both localized joint movement and dynamic full-body motions.

The proposed sensor platform demonstrates reliable and highly directional strain sensing performance under both uniaxial cyclic loading and dynamic body motions. These findings lay a strong groundwork for advancing wearable piezo-transmittance strain sensors toward practical applications that demand robust, precise, and direction-aware motion monitoring.

2 | Results

The conceptual framework, fabrication process, and operational principle of the direction-aware piezo-transmittance strain sensor are illustrated in Figure 1. To overcome the inherent randomness of crack propagation in conventional strain sensors, we designed a structure capable of forming controlled, uniform gaps upon mechanical deformation, as shown in Figure 1A. This concept is realized by inducing a domino-like collapse of CNT films, creating a predictable and directional gap-opening mechanism under applied strain. Figure 1B details the fabrication process developed to achieve this structure (optical photographs corresponding to each step are provided in Figure S1). Vertically aligned CNT arrays are first grown on a silicon substrate via chemical vapor deposition (CVD) [32, 33] (Figure S1A), and then horizontally realigned through a nanostructure rolling system (NRS) into continuous, densely packed CNT sheets (Figure S1B). These horizontally oriented CNT layers are subsequently embedded within a PDMS matrix using a transfer and spin-coating process, forming a flexible composite with engineered directional responsiveness (Figure S1C). The mechanical behavior of the composite under strain is presented in Figure 1C. In the unstrained state, the CNT sheets remain tightly packed without visible gaps. When strain is applied in the transverse direction (perpendicular to the rolling direction), the alignment of CNT sheets prevents noticeable gap formation. In contrast, when tensile strain is applied along the rolling direction, periodic gaps appear between adjacent CNT sheets, allowing light to pass through the composite. This anisotropic gap-opening behavior enables the sensor to distinguish the direction of applied strain based on the transmitted optical signal. Figure 1D illustrates how the anisotropic mechanical response of the CNT–PDMS composite can be extended to realize a direction-aware sensing platform. Independent x- and y-axis sensors are combined into a single device to enable detection of strain along multiple directions. The unstrained state shows both sensors intact with no gap formation, whereas the strained state demonstrates gap opening within the composite, representing the operational principle of the integrated direction-aware sensor. Although only the overall deformation is depicted here, directional dependence arises when each axis-specific sensor responds predominantly to strain applied along its aligned direction.

The effect of CNT aspect ratio on the sensor performance was systematically investigated, as summarized in Figure 2. Here, the aspect ratio is defined as the vertical growth height of CNT arrays relative to their lateral spacing. Three aspect ratios (1:1, 4:1, and 8:1) were examined to evaluate structural alignment, mechanical stretchability, and optical sensitivity. In Figure 2A, SEM images show vertically grown CNT arrays immediately after

2365709x, 2026, 18, Downloaded from https://advanced.onlinelibrary.wiley.com/doi/10.1002/admt.71130 by Korea University Library, Wiley Online Library on [22/09/2026]. See the Terms and Conditions (https://onlinelibrary.wiley.com/terms-and-conditions) on Wiley Online Library for rules of use; OA articles are governed by the applicable Creative Commons License

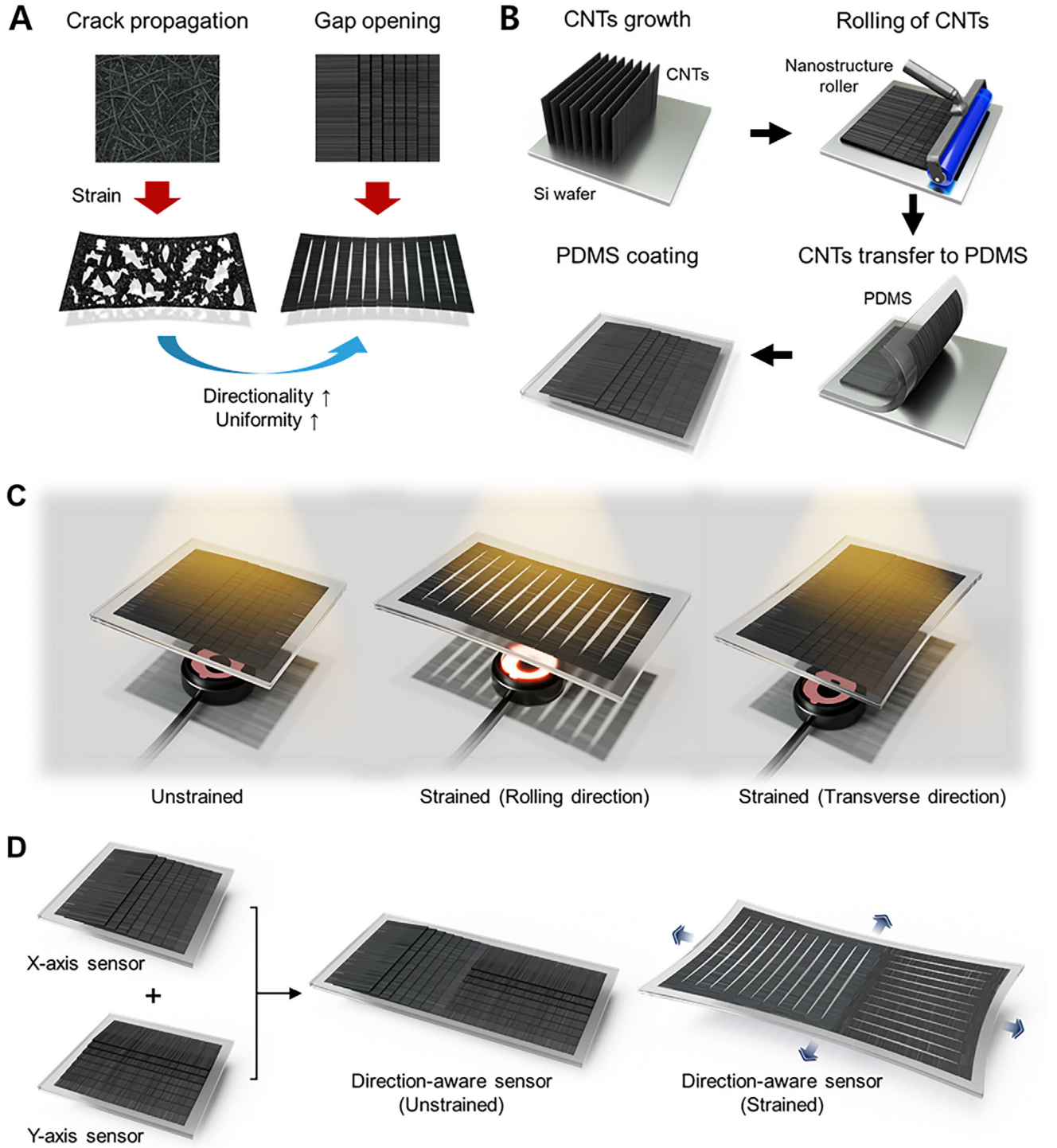


FIGURE 1 | The concept of a direction-aware piezo-transmittance strain sensor with a composite of aligned carbon nanotubes (CNTs) and polydimethylsiloxane (PDMS). (A) Conceptual illustration comparing crack propagation-based piezo-transmittance strain sensors with sensors utilizing a uniform linear gap-opening pattern. (B) Fabrication process of the composite material, CNTs embedded in PDMS matrix, as a precursor to sensor production. (C) Schematic representation of direction-specific crack formation enabled by the uniform linear pattern of the composite under strain, highlighting the sensor's direction-aware response. (D) Assembly of x- and y-axis sensors into a direction-aware strain sensor, showing unstrained and strained states with directional deformation.

the CVD process. Both the 1:1 and 4:1 groups exhibit relatively uniform vertical alignment with coherent structures, whereas the 8:1 group, despite its greater height, displays significant tilting and structural instability, indicating weak vertical coherence. Following the nanostructure rolling process (Figure 2B), differences in horizontal alignment are more pronounced. The 1:1 group, due to its limited initial height, leaves noticeable voids between adjacent CNT sheets after rolling, resulting in incomplete coverage. In contrast, the 8:1 group achieves full coverage without noticeable voids but suffers from irregular, misaligned

2365709x, 2026, 18, Downloaded from https://advanced.onlinelibrary.wiley.com/doi/10.1002/admt.71130 by Korea University Library, Wiley Online Library on [22/09/2026]. See the Terms and Conditions (https://onlinelibrary.wiley.com/terms-and-conditions) on Wiley Online Library for rules of use; OA articles are governed by the applicable Creative Commons License

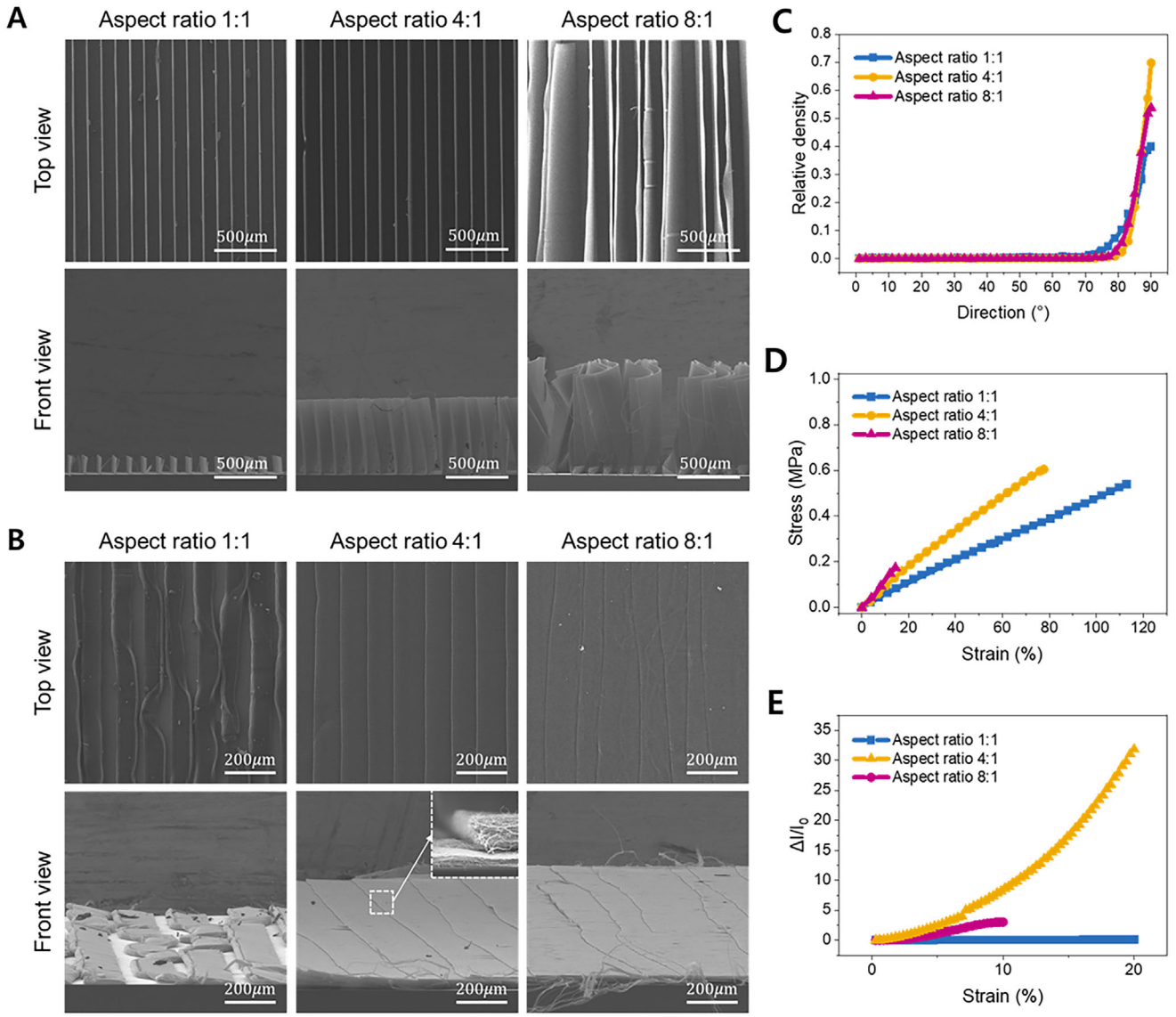


FIGURE 2 | Effect of carbon nanotube (CNT) aspect ratio on alignment uniformity, stretchability, and sensitivity of the strain sensor. (A) SEM images of CNTs grown on Si wafer substrates via the chemical vapor deposition (CVD) process, categorized into three groups with aspect ratios of 1:1, 4:1, and 8:1, all having a pitch of 100 μm. (B) SEM images of CNTs after the nanostructure rolling process, showing structural transformations. (C) Evaluation of directionality in boundaries formed by overlapping nanostructure-rolled CNTs for the three aspect ratio groups. (D) Stress-strain (S-S) curves of nanostructure-rolled CNTs samples coated with polydimethylsiloxane (PDMS) in the elastic deformation region for the three aspect ratio groups. (E) Relative light intensity change ($\Delta I/I_0$) as a function of strain for the three aspect ratio groups.

rolling boundaries, leading to poor overall uniformity. The 4:1 group achieves the most consistent and densely packed horizontal alignment without noticeable voids and with well-ordered sheet boundaries. To quantitatively analyze the directional alignment, an angular distribution histogram of the structural boundaries in Figure 2B was calculated using ImageJ software, as presented in Figure 2C. Herein, the relative density is defined as the normalized frequency of these extracted boundary pixels aligned along each specific angle. Based on this distribution, structures with relative density values strongly concentrated (e.g., close to 90%) exhibit better directional alignment, while greater deviations correspond to increased structural disorder. The 4:1 group maintains a distribution closest to the ideal, further supporting its superior structural integrity. Mechanical stretchability of the different groups is compared in Figure 2D. Both the 1:1 and 4:1 groups exhibit stable and high stretchability, providing sufficient mechanical flexibility for practical applications. In contrast, the 8:1 group exhibits brittle failure even at low strain levels due to excessive overlapping and interlocking of CNT films, severely limiting its mechanical durability. It should be noted that the maximum strain value depicted for each specific group in the stress-strain curves represents the point of complete structural fracture, beyond which the aligned network undergoes irreversible damage. Figure 2E presents the optical sensitivity of the sensors as a function of strain. The 8:1 group initially shows measurable sensitivity but rapidly loses functionality even under small deformations due to early mechanical failure. The 1:1 group, on the other hand, shows limited sensitivity changes because of the high baseline transmittance through its sparsely connected CNT network, diminishing the relative optical modulation upon

2365709x, 2026, 18, Downloaded from https://advanced.onlinelibrary.wiley.com/doi/10.1002/admt.71130 by Korea University Library, Wiley Online Library on [22/09/2026]. See the Terms and Conditions (https://onlinelibrary.wiley.com/terms-and-conditions) on Wiley Online Library for rules of use; OA articles are governed by the applicable Creative Commons License

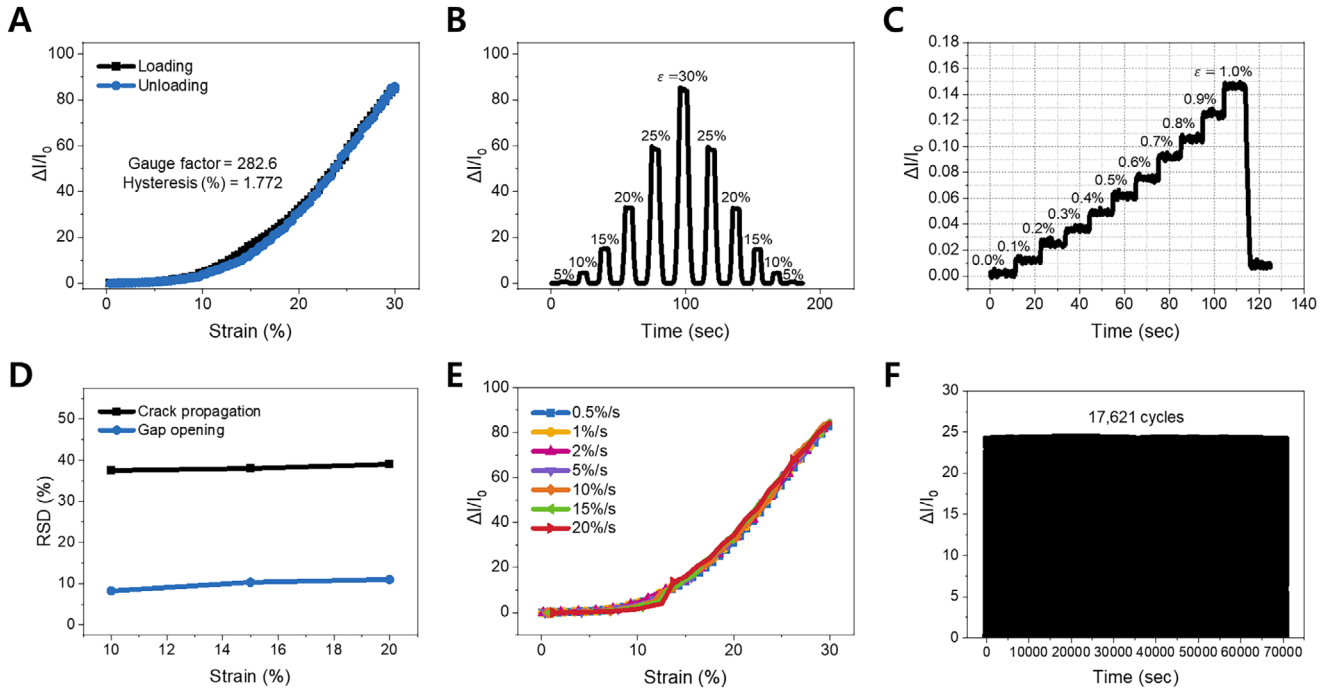


FIGURE 3 | Characterization of the strain sensor. (A) Relative intensity change ($\Delta I/I_0$) during loading and unloading cycles for strains ranging from 0% to 30%, along with evaluations of gauge factor and hysteresis. (B) Relative intensity change ($\Delta I/I_0$) under dynamic strain conditions during cyclic loading. (C) Relative intensity change ($\Delta I/I_0$) under small strain variations, showcasing sensitivity at low deformation levels. (D) Relative standard deviation (RSD) values calculated from the strain-response data in the 10%–20% strain range. (E) Relative intensity change ($\Delta I/I_0$) under different strain rates, showing little influence of strain rate on the sensor performance. (F) Long-term macroscopic stability test results over 17,621 cycles, demonstrating highly consistent relative optical intensity change ($\Delta I/I_0$) and a stable baseline under repeated cyclic loading.

strain. The 4:1 group again achieves optimal performance, maintaining consistent and high sensitivity across the entire strain range. Overall, the 4:1 aspect ratio provides the best compromise among structural uniformity, mechanical stretchability, and optical sensitivity, validating its selection as the optimal configuration for the direction-aware piezo-transmittance strain sensor.

Having established the optimal 4:1 aspect ratio for the sensor's structure (Figure 2), we performed a detailed characterization of its mechanical and sensing performance, as presented in Figure 3. Figure 3A presents the sensor response, measured as the relative intensity change ($\Delta I/I_0$), during loading and unloading over a strain range of 0% to 30%. The $\Delta I/I_0$–strain curve shows a smooth, non-linear increase, with minimal hysteresis between the loading and unloading paths. The sensor achieved a high gauge factor of 282.6 (at 30% strain). Note that due to the non-linear gap-opening behavior, the gauge factor in the initial strain regime (0%–10%) is relatively lower (approx. 30) compared to the higher strain regime. Meanwhile, the hysteresis of 1.772% indicates negligible energy dissipation during cyclic deformation. Dynamic strain sensing stability is evaluated in Figure 3B, where cyclic strain tests from 5% to 30% (in 5% increments) are applied sequentially. The consistent peak heights and sharp recovery after each cycle confirm that the sensor reliably detects varying strain magnitudes without performance degradation, even under multiple sequential loading events. To evaluate the real-time tracking fidelity under high-speed dynamic stimuli, the delay time (Δt) between the mechanical strain input and the sensor response was investigated at a strain rate of 150%/s. This delay time provides a rigorous assessment of the sensor's ability to instantaneously resolve rapid mechanical deformations. As shown in Figure S2, the loading delay and unloading delay were measured to be 72 and 15 ms, respectively, at the 50% threshold of the maximum amplitude. These minimal delay values indicate that the microscopic 3D CNT networks can split and re-contact almost instantaneously upon mechanical deformation, effectively bypassing the inherent viscoelastic lagging typically observed in polymer-based sensors. The sensitivity of the sensor at low strain levels is highlighted in Figure 3C. Incremental strain steps from 0.1% to 1.0% produce clear, stepwise increases in $\Delta I/I_0$, demonstrating the sensor's ability to resolve very small strain changes. The precise response at sub-percent strain levels suggests suitability for applications requiring fine-motion detection. Further analysis of the 0%–0.5% strain region (Figure S3) enables calculation of the sensor's limit of detection (LOD), determined to be approximately 0.03%. This ultra-low LOD underscores the sensor's capability for highly precise strain monitoring in low-deformation scenarios. Figure 3D shows the relative standard deviation (RSD) values calculated from strain-response data in the 10%–20% strain range. The proposed gap-opening sensor achieves RSD values between 7% and 12%, substantially lower than the ~40% RSD observed for conventional crack-propagation-based sensors. The RSD values in Figure 3D are derived from strain-response data across five independently fabricated sensors, as presented in Figure S4, confirming the excellent reproducibility of the sensing performance and the uniformity achieved through the engineered structural design. The rate-dependent electromechanical response of the sensor is examined in Figure 3E. Across various stretching velocities ranging from 0.5%/s to 20%/s, the $\Delta I/I_0$ response curves nearly overlap. This highly consistent behavior

2365709x, 2026, 18, Downloaded from https://advanced.onlinelibrary.wiley.com/doi/10.1002/admt.71130 by Korea University Library, Wiley Online Library on [22/09/2026]. See the Terms and Conditions (https://onlinelibrary.wiley.com/terms-and-conditions) on Wiley Online Library for rules of use; OA articles are governed by the applicable Creative Commons License

confirms that the sensor's sensitivity is independent of the applied strain rate, ensuring reliable performance under dynamic and variable-speed motion conditions. Furthermore, the intrinsic robustness of the sensing mechanism is validated under various baseline light intensities, as detailed in Figure S5. The results confirm that the ΔI/I0 remains highly stable and independent of the baseline optical power ranging from 6.12×10^{-6} to 2.77×10^{-5} W, which ensures consistent and reliable performance across different illumination environments. Collectively, these results highlight the overall robustness of the sensing mechanism against both dynamic mechanical variations (strain rate) and external environmental disturbances. Finally, the long-term durability of the sensor is investigated in Figure 3F. After a severely prolonged test of 17,621 cycles of repeated loading and unloading, the sensor maintains a highly stable macroscopic $\Delta I/I_0$ response without any noticeable baseline drift. Furthermore, magnified dynamic sensing waveforms (Figure S6) reveal that despite a negligible decrease in the maximum signal amplitude (~5%) primarily attributed to the natural stress relaxation of the PDMS, the highly consistent waveform shape is perfectly preserved. To verify the microstructural origin of this longevity, cross-sectional scanning electron microscopy (SEM) analysis was performed. As illustrated in Figure S7, the interface between the aligned CNT network and the PDMS substrate remained intact without any delamination after 10,000 stretching-releasing cycles. Notably, the cross-sectional morphology of the cycled sensor was identical to that of the fresh sample. This observation demonstrates that the robust conformal adhesion is preserved without structural degradation or fatigue-induced failure, fundamentally underpinning the highly reproducible sensing performance. Overall, the characterization results highlight the superior performance of the direction-aware piezo-transmittance strain sensor, demonstrating high sensitivity with minimal hysteresis, excellent sensing reliability under dynamic and cyclic conditions, and outstanding long-term durability. These attributes collectively suggest that the sensor is highly suited for precise and robust strain monitoring in dynamic and wearable environments.

Building upon the established directional sensing capability, Figure 4 explores the multi-directional strain detection performance of the developed sensor. Figure 4A reveals the angle-dependent strain responses when mechanical deformation is applied at different directions relative to the CNT alignment. As the applied strain deviates from the principal rolling (gap-opening) direction, the magnitude of optical transmittance change systematically decreases, confirming the sensor's clear anisotropic sensitivity. Notably, the highest $\Delta I/I_0$ values are observed at 0°, where strain aligns perfectly with the gap-opening orientation, while the response gradually diminishes with increasing misalignment, reaching near-zero at 90°. This directional dependence is further quantified in Figure 4B, which compares gauge factors across different alignment angles. The gauge factor shows a pronounced peak at 0°—which corresponds to the maximum sensitivity (gauge factor ≈ 283) established in Figure 3A—correlating directly with the gap-opening mechanism, and falls sharply beyond 45°, reflecting the mechanical and optical anisotropy engineered into the sensor design. To achieve independent detection of strains along orthogonal axes, a multi-directional sensing structure was fabricated by orthogonally arranging two sensors, as shown in Figure 4C. The SEM image highlights the precise orthogonal configuration of the aligned CNT structures, laying the groundwork for independent strain detection along the x- and y-axes. Figure 4D,E experimentally validate the selective response of the dual-axis configuration. When strained along the x-axis (Figure 4D), the x-axis sensor exhibits a strong periodic $\Delta I/I_0$ signal corresponding to gap opening, while the y-axis sensor remains largely unresponsive. Conversely, when strain is applied along the y-axis (Figure 4E), the y-axis sensor produces a distinct optical signal, whereas the x-axis sensor shows negligible change. These orthogonal responses emphasize the excellent directional specificity and mechanical decoupling achieved by the sensor design. Finally, Figure 4F characterizes the directional response of the sensor by mapping the outputs from both axes in a polar coordinate system. The combined x- and y-axis signals form a clear and predictable pattern, enabling precise determination of arbitrary strain directions based solely on optical transmittance changes. This multi-dimensional sensing capability positions the developed sensor as a promising platform for real-time, angle-resolved mechanical deformation analysis. Overall, these results highlight the sensor's strong directional sensitivity and reliable multi-axis discrimination. To contextualize this performance, Table S1 provides a quantitative benchmark against recently reported multi-directional and direction-aware strain sensors. The comparison clearly demonstrates that our engineered gap-opening mechanism effectively overcomes the inherent trade-offs prevalent in existing technologies. Specifically, the data reveals that while existing piezocapacitive sensors are fundamentally limited in sensitivity (gauge factor < 5), highly sensitive piezoresistive types frequently struggle with significant hysteresis. By resolving these structural bottlenecks, our advanced direction-aware platform achieves an unprecedented balance of ultra-high sensitivity (gauge factor ≈ 283) and strictly quantified minimal hysteresis (1.772%). This performance positions the developed sensor as a highly reliable solution for precise and real-time strain monitoring in wearable applications such as fitness tracking and rehabilitation devices.

The practical integration of the developed direction-aware piezo-transmittance strain sensor into a wearable strain monitoring system, including direct body attachment and incorporation into stretchable exercise bands, is demonstrated in Figure 5. To ensure signal integrity in practical wearable applications where ambient light often fluctuates, the system incorporates a dual-cell configuration for real-time interference cancellation (Figure 5A). Specifically, the architecture utilizes a reference solar cell and a sensing solar cell overlaid with a CNT/PDMS composite, both configured on an Arduino Nano 33 IoT platform. This setup allows the system to perform real-time calibration, ensuring that the output signal exclusively reflects the mechanical strain-induced changes in optical transmittance. This differential measurement strategy effectively decouples the sensing signal from external optical noise, providing consistent monitoring under dynamic lighting conditions. Wearable application scenarios are illustrated in Figure 5B. The flexible and lightweight sensor can be directly attached to body joints, such as the elbow or knee, to monitor localized strain during physical activities, or incorporated into stretchable exercise bands to capture complex multi-directional strain events during dynamic movements. These configurations highlight the sensor's adaptability for precise monitoring of localized joint movements and dynamic full-body motions. Experimental validation is presented

2365709x, 2026, 18, Downloaded from https://advanced.onlinelibrary.wiley.com/doi/10.1002/admt.71130 by Korea University Library, Wiley Online Library on [22/09/2026]. See the Terms and Conditions (https://onlinelibrary.wiley.com/terms-and-conditions) on Wiley Online Library for rules of use; OA articles are governed by the applicable Creative Commons License

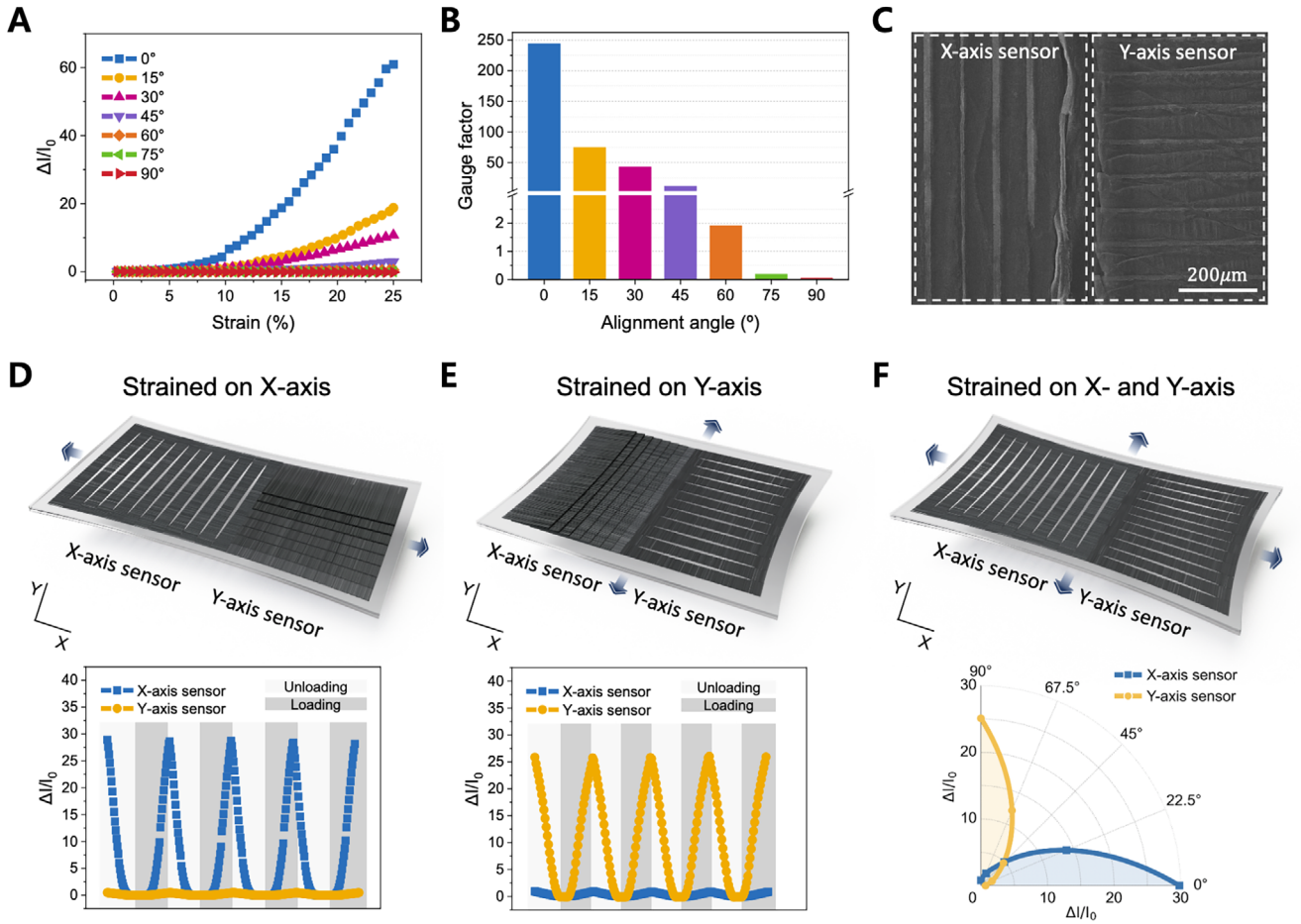


FIGURE 4 | Angle-dependent performance and application of the direction-aware strain sensor. (A) Relative intensity change ($\Delta I/I_0$) under varying strain directions, illustrating angle-dependent variation. (B) Comparison of gauge factors for each group, calculated from the data in (A). (C) Microscopic image of the direction-aware sensor fabricated using two strain sensors arranged perpendicularly for application in directional sensing. (D) Illustration and relative intensity change ($\Delta I/I_0$) showing gap opening when stretched along the x-axis. (E) Illustration and relative intensity change ($\Delta I/I_0$) showing gap opening when stretched along the y-axis. (F) Illustration and polar plot of relative intensity change ($\Delta I/I_0$) showing the selective directional response when strained on both x- and y-axes. The curves represent the sensitivity of the x-axis (blue) and y-axis (yellow) sensors.

in Figure 5C,D. In Figure 5C, the sensor was mounted on the elbow and subjected to repeated bending motions during push-up exercises. The analog signals from the reference and sensing solar cells (Figure 5C-ii) display stable, cyclic variations synchronized with arm motion, while the calculated strain values (Figure 5C-iii) show periodic changes corresponding to the elbow's flexion and extension, demonstrating the system's capability for high-resolution joint motion tracking. Similarly, knee motion during squat exercises was monitored using the sensor attached to the knee joint (Figure 5D-i). The recorded analog signals (Figure 5D-ii) and derived strain curves (Figure 5D-iii) exhibit consistent cyclic behavior, reflecting the dynamic loading and unloading of the knee during repeated squatting motions. These results confirm the sensor's mechanical robustness and signal stability under continuous dynamic deformation.

To further assess the directional sensing capability of the bidirectionally aligned sensor, we mounted it onto a stretchable exercise band, which enabled free application of strain along different directions, including both the x- and y-axes. Photographs of the experimental setups are shown in Figure 5E, where the band was strained to evaluate axis-specific sensor responses. In the x-axis stretching scenario, strain was applied parallel to the CNT alignment direction of the sensing element integrated with solar cell 1. As shown in the measured analog signals (Figure 5F-i), sensing solar cell 1 exhibits distinct periodic responses, while sensing solar cell 2 remains largely unchanged. The calculated strain values (Figure 5F-ii) further validate this direction-selective behavior, with clear strain signals appearing only along the x-axis alignment. In contrast, when the band was stretched along the y-axis, the strain engaged sensing solar cell 2. The corresponding analog outputs (Figure 5G-i) show signal fluctuations exclusively from solar cell 2, and the derived strain curve (Figure 5G-ii) confirms a selective response in the y-axis direction. These results demonstrate the sensor's inherent ability to resolve orthogonal strain directions using spatially separated solar cells and a multi-directionally responsive composite layer. Such directional decoupling enables precise tracking of complex strain patterns in wearable systems, particularly for multi-directional motion detection during physical activity. Overall, the results presented in Figure 5 validate the sensor's versatility, sensitivity, and practical applicability for real-time monitoring of complex human motions in wearable fitness and rehabilitation systems.

2365709x, 2026, 18, Downloaded from https://advanced.onlinelibrary.wiley.com/doi/10.1002/admt.71130 by Korea University Library, Wiley Online Library on [22/09/2026]. See the Terms and Conditions (https://onlinelibrary.wiley.com/terms-and-conditions) on Wiley Online Library for rules of use; OA articles are governed by the applicable Creative Commons License

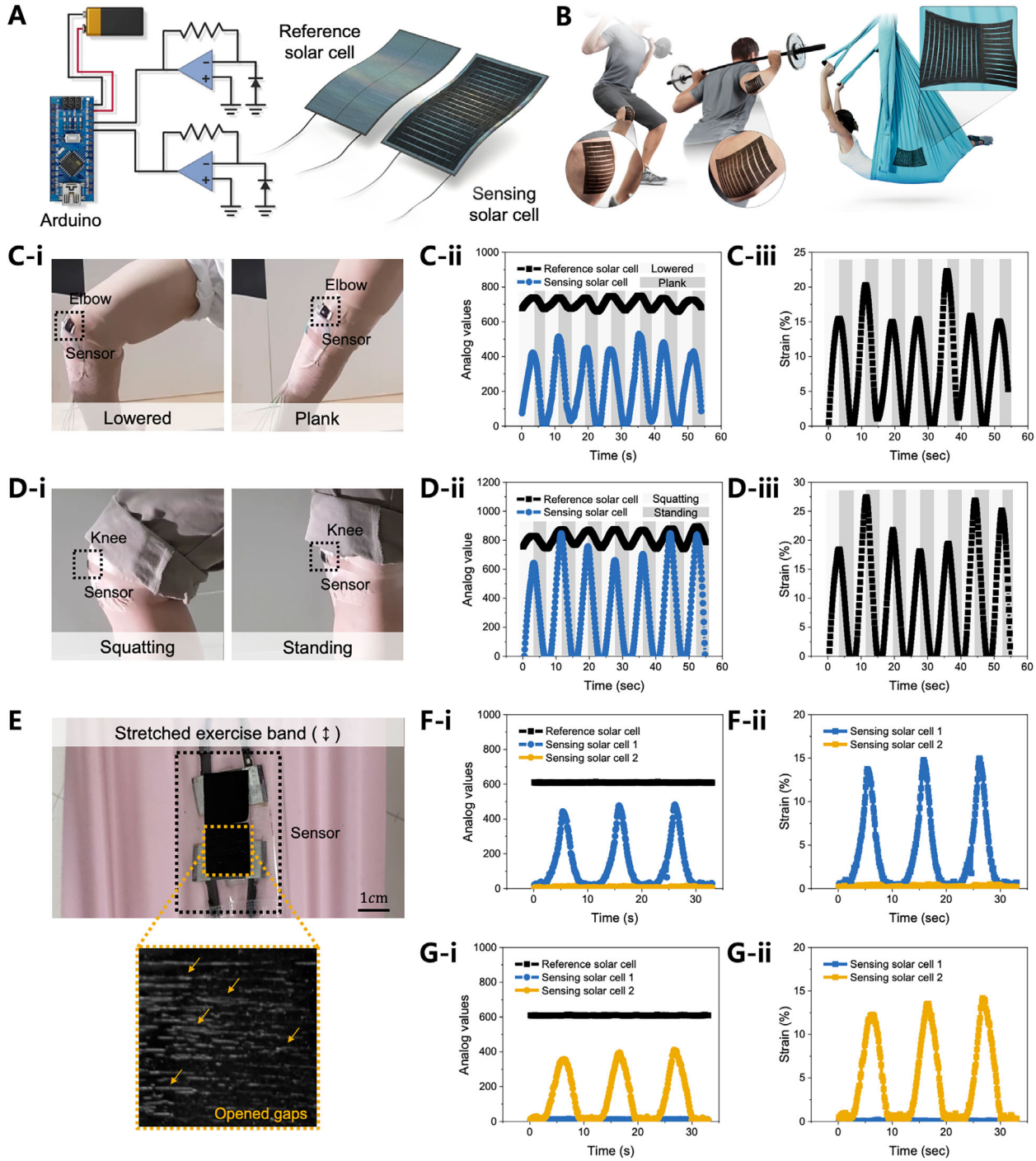


FIGURE 5 | Application of the direction-aware strain sensor for human motion monitoring. (A) Circuit diagram showing the use of the aligned carbon nanotubes (CNTs)/polydimethylsiloxane (PDMS) composite and solar cells for strain sensing in wearable devices. (B) Illustrative examples of wearable applications, showing the sensor attached to the elbow and knee joints or integrated into a stretchable exercise band. (C-i) Photographs showing the plank and lowered positions during push-up motions with the sensor worn on the elbows. (C-ii) Analog values from the reference solar cell and sensing solar cell embedded in the sensor, recorded over time during repeated push-up motions. (C-iii) Strain values calculated from the analog values in (C-ii) and plotted over time. (D-i) Photographs showing the standing and squatting positions during squat motions with the sensor worn on the knees. (D-ii) Analog values from the reference solar cell and sensing solar cell embedded in the sensor, recorded over time during repeated squat motions. (D-iii) Strain values calculated from the analog values in (D-ii) and plotted over time. (E) Photograph of the sensor-integrated exercise band under applied tension. The enlarged view reveals the 'opened gaps' within the aligned CNT/PDMS composite, demonstrating the proposed sensing mechanism. (F) Response of the sensor-integrated exercise band during stretching along the x-axis. (F-i) Analog signals from the reference and sensing solar cells during x-axis stretching. (F-ii) Calculated strain from the signals in (F-i), showing a selective response from the x-axis sensor. (G) Response of the band during stretching along the y-axis. (G-i) Analog signals from the reference and sensing solar cells during y-axis stretching. (G-ii) Calculated strain from the analog signals in (G-i), confirming a selective response in the y-axis sensor.

2365709x, 2026, 18, Downloaded from https://advanced.onlinelibrary.wiley.com/doi/10.1002/admt.71130 by Korea University Library, Wiley Online Library on [22/09/2026]. See the Terms and Conditions (https://onlinelibrary.wiley.com/terms-and-conditions) on Wiley Online Library for rules of use; OA articles are governed by the applicable Creative Commons License

3 | Conclusion

In this study, we developed a direction-aware piezo-transmittance strain sensor by engineering aligned CNTs within a PDMS matrix. By introducing a controlled gap-opening mechanism, the sensor overcame the randomness of traditional crack-based sensors, achieving high sensitivity (gauge factor ≈ 283), low hysteresis (1.772%), strong sensor-to-sensor uniformity (RSD < 12%), an ultra-low detection limit (0.03%), and robust cyclic durability over 17,621 strain cycles. Practical utility was demonstrated through localized joint monitoring and integration with stretchable exercise bands.

Despite these achievements, further optimization is required for reliable signal acquisition. Future work will focus on enhancing the skin-conformability of the elastomer to mitigate slip-induced artifacts during dynamic movements. Furthermore, extending our current orthogonal sensing capability to a three-element strain rosette configuration (e.g., 0°, 45°, and 90°) will overcome inherent symmetric ambiguities. This integration will definitively decouple the exact magnitude and angle of complex multi-directional motions, significantly expanding the application range. Alongside this, investigating the non-linear mechanical coupling induced by the Poisson effect under simultaneous biaxial stretching remains an important task to further refine our strain decoupling models. Finally, while the current dual-cell configuration effectively compensates for ambient light, integrating these components into a fully stretchable optoelectronic module remains a key goal for ultimate wearability.

This work confirms that precise anisotropic alignment is a critical design strategy for high-performance strain sensing. By advancing mechanical fidelity and system-level integration, this technology provides a scalable platform for next-generation wearable electronics, robotics, and personalized healthcare monitoring.

4 | Materials and Methods

4.1 | Materials

The materials used in this study include photoresist (PR; AZ GXR-601, 14 cP; Merck KGaA, Germany), SiO_2-coated silicon substrates (6″, 3000 Å, wet; Silicon Technology Corp., Japan), Fe catalyst (99.99%, 1–3 mm pellet; Taewon Scientific Co., Ltd., Republic of Korea), Al_2O_3 support layer (99.99%, 1–3 mm pellet; Taewon Scientific Co., Ltd., Republic of Korea), argon gas (99.999%; DONG-A Specialty Gases, Republic of Korea), hydrogen gas (99.999%; DONG-A Specialty Gases, Republic of Korea), ethylene gas (99.95%; DONG-A Specialty Gases, Republic of Korea), polydimethylsiloxane (PDMS) (Sylgard 184; Dow Corning Corp., USA), and petri dishes (80 mm × 15 mm, crystal-grade polystyrene; SPL Life Sciences Co. Ltd., Republic of Korea).

4.2 | Fabrication of a Composite Using Aligned Carbon Nanotubes (CNTs) and PDMS

The fabrication process of the composite structure, consisting of directionally aligned CNTs embedded in a PDMS matrix, involved three key stages: (i) growth of aligned CNTs via chemical vapor deposition (CVD), (ii) transformation into a thin-film architecture through a nanostructure rolling process, and (iii) PDMS encapsulation for stretchable integration.

The process began with the patterning of a PR layer on a SiO_2-coated substrate (3000 Å, wet) using photo roll lithography (PRL), performed with a custom-built photolithography system (NcoreTechnology, Inc., Republic of Korea). In the PRL system, a collimated UV light is placed inside a hollow quartz roll, which has a narrow slit (~1 mm wide) to direct the UV light outward. A flexible photomask is attached to the outer surface of the roll, enabling the patterned UV light to be projected onto the moving PR-coated substrate. This configuration ensures continuous and uniform patterning. The detailed PRL methodology has been reported elsewhere [32].

Following PR patterning, a 2-nm Fe catalyst layer and a 10-nm Al_2O_3 support layer were sequentially deposited using an e-beam evaporator (Sci-En Tech Co. Ltd., Republic of Korea) under a base pressure of ~10^{-7} Torr with a 6 kW sweep. A lift-off process was then used to define the catalyst patterns. The growth of vertically aligned CNT arrays, with an intertube spacing of approximately 100 nm, was performed in a CVD system (Sci-En Tech Co. Ltd., Republic of Korea) within a 2-inch quartz tube reactor at atmospheric pressure (Figure S8). The process started with chamber stabilization via argon purging (1000 sccm, 15 min, room temperature), followed by thermal annealing (750°C, 4 min, 300 sccm Ar, 120 sccm H_2) to induce the formation of Fe nanoparticles on the Al_2O_3 surface, which served as nucleation sites for CNT growth. The aligned CNTs were synthesized by introducing a carbon source gas mixture (750°C, 300 sccm Ar, 120 sccm H_2, 90 sccm C_2H_4) for controlled durations of 2 min, 7 min 30 s, and 15 min, determining the final CNT lengths.

The vertically grown CNT structure was then mechanically transformed into a 2D thin film using a nanostructure rolling system (NRS) [34]. The system consists of a three-degree-of-freedom precision stage, a roller-mounted arm for horizontal motion, and a servo motor-controlled mechanism (Figure S9). The CNT structure is placed on the stage, where a controlled force is applied via a roller of predefined diameter and material. Precise parallel alignment between the rolling plane and the substrate surface ensures the uniform formation of the CNT thin film. The details of the NRS procedure were previously reported elsewhere [35], and the mechanical deformation process is visualized in Video S1.

To fabricate a flexible and stretchable composite, the aligned CNT thin film was encapsulated within a PDMS matrix. The PDMS base and curing agent were mixed at a 10:1 mass ratio and degassed in a vacuum chamber for 30 min to eliminate air bubbles. The degassed PDMS was then poured onto a pre-cleaned petri dish and spin-coated at a speed range of 300–400 rpm for 60 s. Excess PDMS was removed via centrifugal force to ensure a reproducible thickness. The coated PDMS was cured on a hotplate at 80°C for 7 h 30 min, forming the first PDMS layer.

After curing, the CNT thin film was transferred onto the PDMS layer by bringing the SiO_2 substrate into contact with the PDMS

2365709x, 2026, 18, Downloaded from https://advanced.onlinelibrary.wiley.com/doi/10.1002/admt.71130 by Korea University Library, Wiley Online Library on [22/09/2026]. See the Terms and Conditions (https://onlinelibrary.wiley.com/terms-and-conditions) on Wiley Online Library for rules of use; OA articles are governed by the applicable Creative Commons License

surface, applying moderate pressure, and gently peeling off the SiO_2 layer. A second PDMS layer, fabricated using the same process, was then applied to fully encapsulate the CNT thin film. Finally, the composite structure was carefully trimmed to achieve precise dimensions and remove excess PDMS, ensuring a clean and uniform device suitable for stretchable and wearable applications.

4.3 | Characterization of the Piezo-Transmittance Strain Sensor

To evaluate the mechanical properties of the CNT/PDMS composite films, a universal testing machine (AGS-X plus series, Shimadzu, Japan) was employed to perform stress-strain tests. For optical transmittance measurements, a separate setup was used, in which the sensor samples were mounted onto a customized uniaxial linear stage where controlled tensile strains were applied. A solar illuminator (LAX-C100 Xenon light source, Asahi Spectra Co., Ltd., Japan) emitting visible light in the wavelength range of 400–800 nm was positioned above the sample to provide uniform illumination. The transmitted light through the sample was detected by an optical power sensor (S120C, Thorlabs, USA) placed directly beneath the sample, with a detecting area diameter of 9.5 mm. Changes in the transmitted light intensity were recorded to evaluate the strain-dependent optical response of the sensor. A charge-coupled device camera was also used to capture optical images of gap-opening behavior during strain application, allowing visual confirmation of mechanical deformation modes.

4.4 | Human Motion Monitoring Using the Developed Strain Sensor

The human motion monitoring experiments were conducted using a custom-built strain sensing system consisting of a commercial solar cell (ONP1.2–12 × 24, PowerFilm, Inc., USA) as the reference and sensing elements, with the sensing solar cell overlaid by the aligned CNT/PDMS composite and integrated onto an Arduino Nano 33 IoT platform. The output current from the solar cells was converted into voltage signals through a transimpedance amplifier circuit to monitor strain-dependent optical transmittance changes. To simulate a realistic outdoor environment during the experiments, a solar illuminator was used as the ambient light source. Under this illumination, the reference solar cell was exposed to the ambient light, while the sensing solar cell was covered with the aligned CNT/PDMS composite. The strain-induced transmittance changes were detected by measuring the differential signal between the reference and sensing solar cells, allowing calibration against external light variations. To ensure accurate signal conversion and minimize potential baseline fluctuations, the raw analog data ($V_{sensing}$) was first normalized against the reference signal (V_{ref}) and scaled by a predefined correction factor (k). The resulting normalized input ($x = k \cdot \frac{V_{sensing}}{V_{ref}}$) was then mathematically converted into mechanical strain values (%) using a fifth-degree polynomial equation:

$$\epsilon\ (\%) = b_5\, x^5 + b_4 x^4 + b_3 x^3 + b_2 x^2 + b_1 x + b_0$$

where b_n denotes the fitting coefficients meticulously determined through a calibration process using a customized uniaxial linear stage. This high-order polynomial regression model was specifically employed to effectively compensate for the inherent non-linear optical transmittance changes associated with the gap-opening mechanism. Consequently, this rigorous signal processing ensures high-fidelity, highly reliable data acquisition across the entire sensing range during diverse human motion monitoring. For experimental demonstration, the developed sensor system was directly attached to body joints such as the elbow and knee to monitor dynamic human motions. In addition, the sensor was mounted on a commercial stretchable exercise band to track its elongation and recovery during repetitive stretching exercises. All experiments involving human participants were approved by the institutional review board of KAIST (IRB-24-361).

Acknowledgements

This work was supported by the National Research Foundation of Korea (NRF) grant funded by the Korea government (MSIT) (RS-2026-25476229), by the Alchemist Project grant funded by the Korea Evaluation Institute of Industrial Technology (KEIT) and the Korea government (MOTIE) (Project number: 1415179744, 20019169), and by the innoCORE program of the Ministry of Science and ICT (N10260002).

Conflicts of Interest

The authors declare no conflicts of interest.

Data Availability Statement

The data that support the findings of this study are available from the corresponding author upon reasonable request.

References

1. M. Amjadi, K.-U. Kyung, I. Park, and M. S. Sitti, "Stretchable, Skin-Mountable, and Wearable Strain Sensors and Their Potential Applications: A Review," *Advanced Functional Materials* 26, no. 11 (2016): 1678–1698, https://doi.org/10.1002/adfm.201504755.

2. H. Kim, Y.-T. Kwon, H.-R. Lim, J.-H. Kim, Y.-S. Kim, and W.-H. Yeo, "Recent Advances in Wearable Sensors and Integrated Functional Devices for Virtual and Augmented Reality Applications," *Advanced Functional Materials* 31, no. 39 (2021): 2005692, https://doi.org/10.1002/adfm.202005692.

3. Y. Lin, W. Qiu, and D. Kong, "Stretchable and Body-Conformable Physical Sensors for Emerging Wearable Technology," *Sensors & Diagnostics* 3, no. 9 (2024): 1442–1455, https://doi.org/10.1039/D4SD00189C.

4. H. Souri, H. Banerjee, A. Jusufi, et al., "Wearable and Stretchable Strain Sensors: Materials, Sensing Mechanisms, and Applications," *Advanced Intelligent Systems* 2, no. 8 (2020): 2000039, https://doi.org/10.1002/aisy.202000039.

5. Z. Shen, F. Liu, S. Huang, et al., "Progress of Flexible Strain Sensors for Physiological Signal Monitoring," *Biosensors and Bioelectronics* 211 (2022): 114298, https://doi.org/10.1016/j.bios.2022.114298.

6. S. Zhao, D. Liu, and F. Yan, "Wearable Resistive-Type Stretchable Strain Sensors: Materials and Applications," *Advanced Materials* 37, no. 5 (2025): 2413929, https://doi.org/10.1002/adma.202413929.

7. T. Huang, Y. Long, Z. Dong, et al., "Elastic, Hybrid Aerogel for Flexible/Wearable Piezoresistive Sensor and Solid–Solid/Gas–Solid Coupled Triboelectric Nanogenerator," *Advanced Science* 9, no. 34 (2022): 2204519, https://doi.org/10.1002/advs.202204519.

2365709x, 2026, 18, Downloaded from https://advanced.onlinelibrary.wiley.com/doi/10.1002/admt.71130 by Korea University Library, Wiley Online Library on [22/09/2026]. See the Terms and Conditions (https://onlinelibrary.wiley.com/terms-and-conditions) on Wiley Online Library for rules of use; OA articles are governed by the applicable Creative Commons License

8. A. J. Cheng, L. Wu, Z. Sha, et al., "Recent Advances of Capacitive Sensors: Materials, Microstructure Designs, Applications, and Opportunities," *Advanced Materials Technologies* 8, no. 11 (2023): 2201959, https://doi.org/10.1002/admt.202201959.

9. X. Wang, Y. Deng, P. Jiang, X. Chen, and H. L.-H. Yu, "Low-Hysteresis, Pressure-Insensitive, and Transparent Capacitive Strain Sensor for Human Activity Monitoring," *Microsystems & Nanoengineering* 8, no. 1 (2022): 113, https://doi.org/10.1038/s41378-022-00450-7.

10. W. Peng and H. Wu, "Flexible and Stretchable Photonic Sensors Based on Modulation of Light Transmission," *Advanced Optical Materials* 7, no. 12 (2019): 1900329, https://doi.org/10.1002/adom.201900329.

11. P. P. Pancham, W.-H. Chiu, A. Mukherjee, and C.-Y. Lo, "Strain Visualization in Flexible Sensors with Functional Materials: A Review," *Advanced Materials Interfaces* 10, no. 14 (2023): 2300029, https://doi.org/10.1002/admi.202300029.

12. Y. Zhao, J. Hao, Z. Lin, et al., "Triethoxysilane-Enhanced Graphene/Carbon Nanoparticles Conductive Network for Multifunctional Fabric Electronics With Pressure, Temperature and Strain Sensing Capabilities," *Chemical Engineering Journal* 511 (2025): 162254, https://doi.org/10.1016/j.cej.2025.162254.

13. Y. Zhao, S. Mu, B. Hu, et al., "Polyvinyl Alcohol/Silk Fibroin/Graphene Hydrogel-Based Flexible Sensor With Self-Healing, Ultra-Stretchable, and Eco-Friendly Properties for Advanced Wearable Electronics and Human-Machine Interaction Applications," *Sensors and Actuators B: Chemical* 445 (2025): 138566, https://doi.org/10.1016/j.snb.2025.138566.

14. J. Choi, D. Kwon, B. Kim, et al., "Wearable Self-Powered Pressure Sensor by Integration of Piezo-Transmittance Microporous Elastomer With Organic Solar Cell," *Nano Energy* 74 (2020): 104749, https://doi.org/10.1016/j.nanoen.2020.104749.

15. L. Wu, J. Ahn, J. Choi, et al., "Customizable Self-Powered Pressure Sensor Based on Piezo-Transmittance of Tilted Structures," *Nano Energy* 109 (2023): 108299, https://doi.org/10.1016/j.nanoen.2023.108299.

16. G. Lee, J. Choi, J. Ahn, S. Cho, and I. Park, "Piezo-Transmissive Structure Using a Multi-Layered Heterogeneous Film for Optical Transmittance Modulation," *ACS Applied Materials & Interfaces* 15, no. 16 (2023): 20531–20540, https://doi.org/10.1021/acsami.3c01619.

17. Q. Zhai and Y. Yang, "Highly Stretchable Variable-Transmittance Skin for Ultrasensitive and Wearable Strain Sensing," *Advanced Materials Technologies* 2, no. 10 (2017): 1700161, https://doi.org/10.1002/admt.201700161.

18. J. Gu, D. Kwon, J. Ahn, and I. Park, "Wearable Strain Sensors Using Light Transmittance Change of Carbon Nanotube-Embedded Elastomers With Microcracks," *ACS Applied Materials & Interfaces* 12, no. 9 (2020): 10908–10917, https://doi.org/10.1021/acsami.9b18069.

19. Y. Jiang, Y. Wang, Y. K. Mishra, R. Adelung, and Y. Yang, "Stretchable CNTs-Ecoflex Composite as Variable-Transmittance Skin for Ultrasensitive Strain Sensing," *Advanced Materials Technologies* 3, no. 12 (2018): 1800248, https://doi.org/10.1002/admt.201800248.

20. J. Gu, J. Ahn, J. Jung, et al., "Self-Powered Strain Sensor Based on the Piezo-Transmittance of a Mechanical Metamaterial," *Nano Energy* 89 (2021): 106447, https://doi.org/10.1016/j.nanoen.2021.106447.

21. J. Gu, Y. Jung, J. Ahn, et al., "Auxetic Kirigami Structure-Based Self-Powered Strain Sensor With Customizable Performance Using Machine Learning," *Nano Energy* 130 (2024): 110124, https://doi.org/10.1016/j.nanoen.2024.110124.

22. S. Hong, V. P. Rachim, J.-H. Baek, and S.-M. Park, "Real-Time Multiaxial Strain Mapping Using Computer Vision Integrated Optical Sensors," *npj Flexible Electronics* 7 (1) (2023): 30, https://doi.org/10.1038/s41528-023-00264-1.

23. S. Ryu, P. Lee, J. B. Chou, et al., "Extremely Elastic Wearable Carbon Nanotube Fiber Strain Sensor for Monitoring of Human Motion," *ACS Nano* 9, no. 6 (2015): 5929–5936, https://doi.org/10.1021/acsnano.0165b00599.

24. Z. Lu, J. Wang, L. He, J. Song, Z. Yang, and F. A. Hammad, "High-Performance Multidirectional Flexible Strain Sensor for Human Motion and Health Monitoring," *ACS Applied Materials & Interfaces* 16, no. 31 (2024): 41409–41420, https://doi.org/10.1021/acsami.4c04583.

25. Z. Liu, Z. Li, Y. Yi, et al., "Flexible Strain Sensing Percolation Networks Towards Complicated Wearable Microclimate and Multi-Direction Mechanical Inputs," *Nano Energy* 99 (2022): 107444, https://doi.org/10.1016/j.nanoen.2022.107444.

26. M. S. Kim, Y. Lee, J. Ahn, et al., "Skin-like Omnidirectional Stretchable Platform with Negative Poisson's Ratio for Wearable Strain–Pressure Simultaneous Sensor," *Advanced Functional Materials* 33, no. 3 (2023): 2208792, https://doi.org/10.1002/adfm.202208792.

27. S. Wang, Y. Fang, H. He, L. Zhang, C. Li, and J. Ouyang, "Wearable Stretchable Dry and Self-Adhesive Strain Sensors With Conformal Contact to Skin for High-Quality Motion Monitoring," *Advanced Functional Materials* 31, no. 5 (2021): 2007495, https://doi.org/10.1002/adfm.202007495.

28. F. Ershad, A. Thukral, J. Yue, et al., "Ultra-Conformal Drawn-on-Skin Electronics for Multifunctional Motion Artifact-Free Sensing and Point-of-Care Treatment," *Nature Communications* 11, no. 1 (2020): 3823, https://doi.org/10.1038/s41467-020-17619-1.

29. S. Wan, Z. Zhu, K. Yin, et al., "A Highly Skin-Conformal and Biodegradable Graphene-Based Strain Sensor," *Small Methods* 2, no. 10 (2018): 1700374, https://doi.org/10.1002/smtd.201700374.

30. H. Li, Z. Wang, M. Sun, et al., "Breathable and Skin-Conformal Electronics With Hybrid Integration of Microfabricated Multifunctional Sensors and Kirigami-Structured Nanofibrous Substrates," *Advanced Functional Materials* 32, no. 32 (2022): 2202792, https://doi.org/10.1002/adfm.202202792.

31. J. Ahn, T. Kim, J.-H. Ha, et al., "Skin-Conformal Motion Monitoring Film for Deep-Learning-Based Immersive Extended Reality," *Advanced Functional Materials* 35, no. 28 (2025): 2502568, https://doi.org/10.1002/adfm.202502568.

32. H. Roh, K. Kim, C. Kim, et al., "Polymer-Incorporated Mechanically Compliant Carbon Nanotube Microelectrode Arrays for Multichannel Neural Signal Recording," *Advanced Functional Materials* 35 (2025): 2509630, https://doi.org/10.1002/adfm.202509630.

33. K. Kim, J. Park, J. M. Park, and J. G. M. Ok, "Domino-Overlapped CNT Scaffolds Homogeneously Hybridized with BTO-P(VDF-TrFE) for High-Performance Piezoelectric Nanogenerators," *Advanced Functional Materials* 35 (2025): 2523382, https://doi.org/10.1002/adfm.202523382.

34. J. G. Ok, M. K. Kwak, C. M. Huard, H. S. Youn, and L. J. Guo, "Photo–Roll Lithography (PRL) for Continuous and Scalable Patterning With Application in Flexible Electronics," *Advanced Materials* 25, no. 45 (2013): 6554–6561, https://doi.org/10.1002/adma.201303514.

35. J. H. Ahn, M. Na, S. Koo, et al., "Development of a Fully Automated Desktop Chemical Vapor Deposition System for Programmable and Controlled Carbon Nanotube Growth," *Micro and Nano Systems Letters* 7, no. 1 (2019): 11, https://doi.org/10.1186/s40486-019-0091-8.

Supporting Information

Additional supporting information can be found online in the Supporting Information section.

Supporting File 1: admt71130-sup-0001-SuppMat.docx.

Supporting File 2: admt71130-sup-0002-VideoS1.mp4.

2365709x, 2026, 18, Downloaded from https://advanced.onlinelibrary.wiley.com/doi/10.1002/admt.71130 by Korea University Library, Wiley Online Library on [22/09/2026]. See the Terms and Conditions (https://onlinelibrary.wiley.com/terms-and-conditions) on Wiley Online Library for rules of use; OA articles are governed by the applicable Creative Commons License